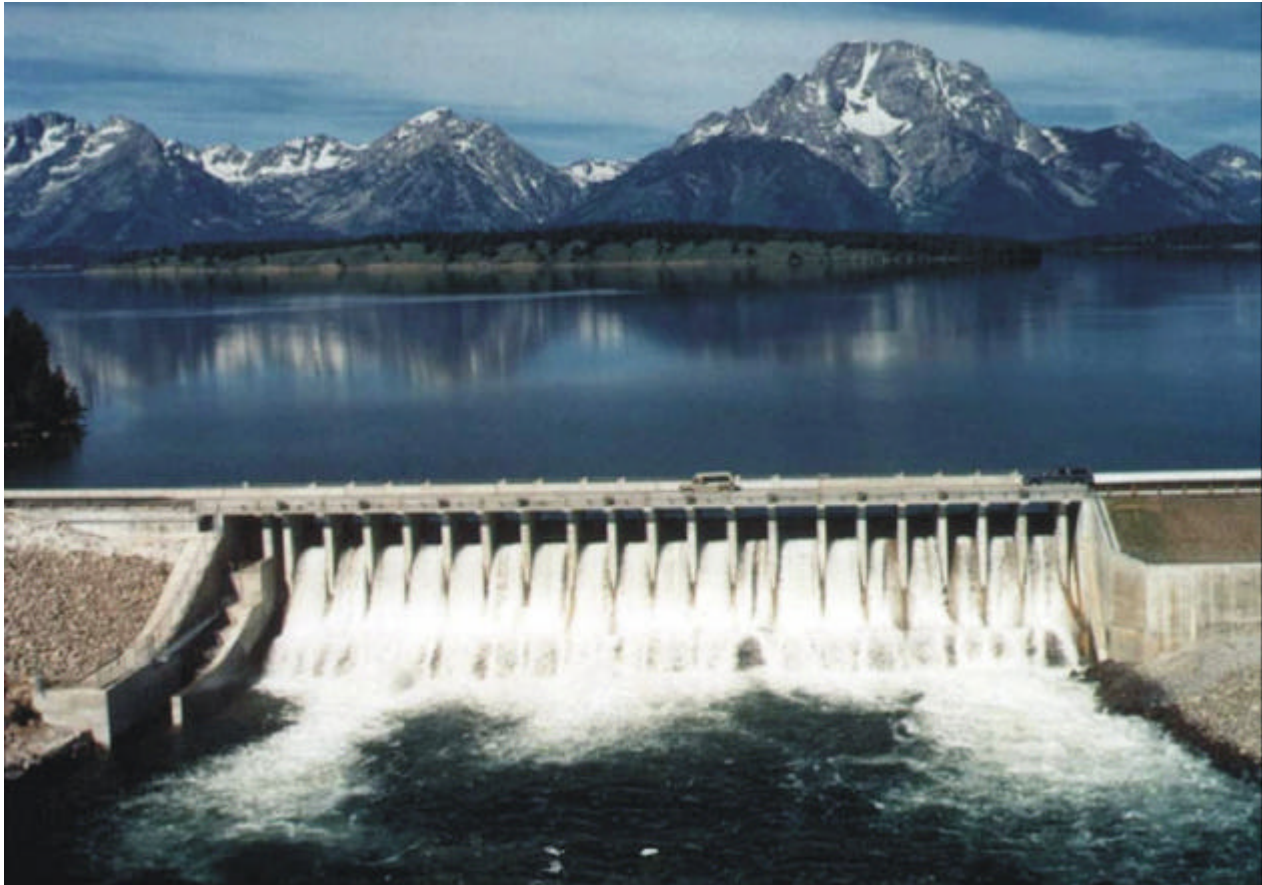


Final Report

Ground Motion Evaluation
for
Jackson Lake Dam
Minidoka Project, Wyoming



Seismotectonics and Geophysics Group
Technical Service Center
Bureau of Reclamation
Denver, Colorado



June 2003

FINAL REPORT

**Ground Motion Evaluation
for
Jackson Lake Dam, Minidoka Project, Wyoming**

Prepared by
Daniel R. H. O'Connell
Christopher K. Wood
Dean A. Ostenaas
Lisa V. Block
Roland C. LaForge

Report 2003-2

Seismotectonics and Geophysics Group
Technical Service Center
Bureau of Reclamation
Denver, Colorado

June 2003



R E C L A M A T I O N ' S M I S S I O N

The mission of the Bureau of Reclamation is to manage, develop, and protect water and related resources in an environmentally and economically sound manner in the interest of the American public.

D E P A R T M E N T O F T H E I N T E R I O R ' S M I S S I O N

The mission of the Department of the Interior is to protect and provide access to our Nation's natural and cultural heritage and honor our trust responsibilities to tribes.

FINAL REPORT

June 13, 2003

Prepared by:

Daniel R.H. O'Connell

June 20, 2003
Date

Christopher K. Wood

June 20, 2003
Date

Dean A. Ostena

June 20, 2003
Date

Lisa V. Block

June 23, 2003
Date

Roland C. LaForge

June 20, 2003
Date

TSC Peer Review by:

Jon P. Ake

June 23, 2003
Date

Larry W. Anderson

June 20, 2003
Date

Table of Contents

<u>Section</u>	<u>Title</u>	<u>Page</u>
	EXECUTIVE SUMMARY.....	III
1.0	INTRODUCTION.....	1
1.1	Introduction	1
1.2	Objectives and Scope	2
1.2.1	Teton Fault Source Characterization	3
1.2.2	Seismicity Analyses	4
1.2.3	Hanging Wall Crustal Velocity Structure	4
1.2.4	Empirical Site Response	4
1.2.5	Ground Motion Estimation for Jackson Lake Dam	5
1.3	Jackson Lake Dam	6
1.3.1	Geologic Setting of the Dam	8
1.3.2	Previous Seismic Hazard and Ground Motion Studies	10
1.4	Acknowledgements	11
2.0	TETON FAULT- SOURCE CHARACTERIZATION.....	13
2.1	Introduction	13
2.1.1	Primary Data Sources	16
2.2	Late Quaternary Faulting on the Teton Fault	17
2.2.1	Quaternary Chronology of Faulted Deposits Along the Teton Fault	17
2.2.2	Distribution of Late Quaternary Fault Scarps and Surface Rupture	20
2.2.2.1	Relationship of the Late Quaternary Fault to Older Structures	25
2.2.2.2	Fault Dip	28
2.2.3	Slip Rate and Along-Strike Variations in Displacement	30
2.2.3.1	Age(s) and Number of Faulting Events	34
2.2.4	Segmentation	36
2.3	Potential Fault Rupture Models	37
2.3.1	Unsegmented, with Variable Displacement Along Strike.	38
2.3.2	Two Independent Fault Segments with Overlapping Rupture.	38
2.3.3	Three Independent Fault Segments.	39
2.3.4	Implications for Ground Motion Models	39
3.0	SEISMICITY ANALYSES	41
3.1	Hypocenter-Velocity-Station Correction Inversion	44
3.1.1	Procedure	44
3.1.2	Improvement in Residuals	45
3.1.3	New Velocity Model and Station Corrections	45
3.1.4	Final Earthquake Locations	49
3.2	Focal Mechanisms	49
3.3	Earthquake Recurrence	61
3.4	Catalog Development	62
3.4.1	Jackson Lake Network Catalog	62
3.4.1.1	Declustering	62
3.4.2	Pre-Jackson Lake Network Catalog	65

3.5	Recurrence Calculations	71
3.6	Earthquake Recurrence Discussion	71
3.7	Summary and Conclusions	80
4.0	HANGING WALL CRUSTAL VELOCITY STRUCTURE.....	85
4.1	3D Velocity Model Development Using Seismic Refraction Data.	87
4.2	3D Velocity Model Development Using LVB Seismograms.	91
4.2.1	Synthetic Seismogram Modeling of the 19 April 2001 M 1.4 Earthquake	92
4.2.2	Synthetic Seismogram Modeling of the 29 Sep. 1996 M 1.6 Earthquake	94
4.2.3	Synthetic Seismogram Modeling of the 15 Nov. 2001 M 2.9 Earthquake	103
4.3	Comparison of 3D Velocity Model to the Seismic Refraction Data	106
4.4	Seismic LVB Responses to Teton Fault Earthquakes: Influence of LVB Structure	109
4.5	Structural Interpretation of Hanging Wall Geology and Geophysics	118
4.6	Conclusions	120
5.0	SITE RESPONSE	125
5.1	Weak-Motion Site Response	125
5.1.1	Instrumented Sites	127
5.1.2	Initial Data Recording System	132
5.1.3	Upgraded Data Recording System	134
5.2	Observations	134
5.2.1	Waveform Data Results	135
5.2.2	Spectral Ratio Method	138
5.2.3	Average Spectral Ratios	139
5.3	Weak-Motion Impulse Response Functions	145
5.3.1	Impulse Response Functions for JLD2 and JLD3	148
5.3.2	Bedrock Motions with Weak-Motion Site Response Included	151
5.4	2D Finite-Difference Site Response Modeling	158
5.4.1	Previous Work	158
5.4.2	Site-Specific Model	160
5.5	Summary and Conclusions.	182
6.0	GROUND MOTION MODELING	185
6.1	Overall Approach	185
6.1.1	Green's Function For Linear Ground Motions.	187
6.1.2	Nonlinear Soil Ground Motions.	187
6.2	Source Parameterization	189
6.3	Linear Wave Propagation Methods	195
6.3.1	Low-Frequency 3D Green's Functions.	195
6.3.1.1	Viscoelastic 3D Finite-Difference Calculations	197
6.3.2	High-Frequency Empirical Green's Functions.	197
6.4	Linear Ground Motion Simulations	206
6.4.1	Idealized Fault Rupture Geometries.	206
6.4.2	Forward Calculations of Low-Frequency 3D Ground Motions.	206
6.4.3	Broadband Hybrid Ground Motions.	216
6.4.3.2	Northern Teton Fault Segment - 35° Dip	218
6.4.3.3	Northern Teton Fault Segment - 45° Dip.	226
6.4.3.4	Northern Teton Fault Segment - 60° Dip.	234

6.4.4	Comparison of Linear Ground Motions for Varying Fault Dips.	238
6.5	Ground Motions for Dynamic Analyses of the Concrete Portion of Jackson Lake Dam.	245
6.6	Inputs for Nonlinear Ground Motion Calculations	264
6.6.1	Nonlinear Compacted Soil Zone Results	275
6.6.2	Nonlinear Soil Mix Wall Results	275
6.6.3	Discussion of Nonlinear Results	282
6.7	Ground Motion Summary	285
7.0	ANALYSIS OF ESTIMATED GROUND MOTIONS.....	291
7.1	Strong Ground Motions From the 1979 M 6.5 Imperial Valley Earthquake	292
7.2	Performance of the Kinematic Rupture Model	305
7.2.1	Validation Ground Motion Modeling Approach: Green's Functions	307
7.2.2	Kinematic Rupture Model Test: Northridge Ground Motions	311
7.3	Alternative Ground Motion Synthesis Approach of Frankel (1995)	330
7.4	Ground Motions From Larger Regional Earthquakes	335
7.4.1	Rock Site JLDW	340
7.4.2	Soil Site JLD3	362
7.5	Ground Motion Synthesis with Local Broadband Empirical Green's Functions	373
7.5.1	Simulated Ground Motions Using the 11 July 1998 M2.9 EGF's	383
7.5.2	Simulated Ground Motions Using the 20 November 2002 M 3.2 EGF	393
7.5.3	Influence of EGF Location on Long-Period Responses	397
7.6	Comparison to Broadband Hybrid Ground Motions From Section 6.	401
7.7	Discussion.	409
8.0	CONCLUSIONS	417
8.1	Teton Fault Slip Rates	418
8.2	Teton Fault Dip	419
8.3	3D Crustal Velocity Structure	420
8.4	Soil Site Response	422
8.5	Ground Motion Estimation	425
8.6	Rock Ground Motions for the Concrete Section	436
8.7	Rock Ground Motion Time Histories	437
8.8	Recommended Acceleration Seismograms for Nonlinear Soil Analyses	450
8.9	Appropriate Use of Ground Motions	453
9.0	REFERENCES.....	459

List of Figures

<u>Figure No.</u>	<u>Title</u>	<u>Page</u>
Figure 1-1:	Map showing location of Jackson Lake Dam and late Quaternary trace of Teton fault.....	2
Figure 1-2:	Schematic sections through Jackson Lake Dam at stations 12+00, 24+00, and 31+00.....	7
Figure 1-3:	Generalized geologic cross section along the axis of Jackson Lake Dam.....	9
Figure 2-1:	Regional tectonic map of the northwestern Wyoming and Jackson Lake Dam region.....	14
Figure 2-2:	Map of the Teton Range-Jackson Hole region showing the generalized late Quaternary trace of the Teton fault in relationship to Jackson Lake Dam.....	15
Figure 2-3:	Map of fault traces defined by late Quaternary fault scarps along the Teton fault.....	22
Figure 2-4:	Schematic geologic cross section of the Teton Range and Jackson Hole depicting a vertical offset of ~6 km on the Teton fault copied from Smith et al. (1993).....	26
Figure 2-5:	Various interpretations of the Teton Range and Teton normal fault from 1938 through 1974 (Figure 6 of Lageson, 1992).....	27
Figure 2-6:	Schematic geologic cross section depicting late Quaternary Teton fault versus basin structure to east of fault.....	28
Figure 2-7:	Estimated vertical slip rates along the Teton fault.....	33
Figure 2-8:	Shoreline intervals for Bearpaw Bay shorelines.....	37
Figure 3-1:	Map showing the distribution of JLSN seismographic stations.....	42
Figure 3-2:	Map showing the distribution of Jackson Lake Dam site-response seismographs.....	43
Figure 3-3:	Histograms of arrival time residuals.....	45
Figure 3-4:	Plan views of P-wave velocities for elevations (relative to mean sea level) of -5 km to 2 km.....	46
Figure 3-5:	Plan view of the final locations of 4642 events relocated in the 3D velocity model from the joint inversion.....	50
Figure 3-6:	Histogram of the final earthquake elevations (with respect to mean sea level, e.g., 0 km).....	51
Figure 3-7:	West-east depth sections of earthquake locations.....	53
Figure 3-8:	T-axes azimuths from the 303 focal mechanisms with < 5° T-axis solution variability.....	54
Figure 3-9:	T-axes azimuths from the 773 focal mechanisms with < 20° T-axis solution variability.....	55
Figure 3-10:	“Pure” nodal planes from focal mechanisms with < 5° T-axis solution variability.....	57
Figure 3-11:	“Pure” strike-slip and oblique dip-slip nodal planes from focal mechanisms with < 5° T-axis solution variability.....	58
Figure 3-12:	“Pure” nodal planes from focal mechanisms with < 20° T-axis solution variability.....	59
Figure 3-13:	“Pure” strike-slip and oblique dip-slip nodal planes from focal mechanisms with < 20° T-axis solution variability.....	60
Figure 3-14:	Epicenters from Jackson Lake Seismic Network, magnitude > 2.0, June	

1986 - December 2001.....	63
Figure 3-15a Latitude vs. time, unfiltered JLSN catalog.....	66
Figure 3-15b Longitude vs. time, unfiltered JLSN catalog	66
Figure 3-16a Latitude vs. time, declustered JLSN catalog.....	67
Figure 3-16b Longitude vs. time, declustered JLSN catalog.	67
Figure 3-17: JLSN earthquakes identified as being clusters by declustering algorithm.	68
Figure 3-18: JLSN earthquakes identified as independent events by declustering algorithm.	69
Figure 3-19: 1963 - June 1986 epicenters, from NCDEC.....	70
Figure 3-20: Declustered earthquakes used in recurrence calculations using the combined catalogs.	72
Figure 3-21a Incremental recurrence curve for JLSN catalog.	74
Figure 3-21b Cumulative recurrence curve for JLSN catalog.	74
Figure 3-22a Incremental recurrence curve for combined catalogs. The ellipse shows the approximate rate of M ~6.7-7.2 earthquakes on the Teton fault based on Section 2	75
Figure 3-22b Cumulative recurrence curve for combined catalogs.	75
Figure 3-23a Example soil-site hazard curves for random seismicity at Jackson Lake Dam.	78
Figure 3-23b Example rock-site hazard curves for random seismicity at Jackson Lake Dam.	78
Figure 4-1: Plan view of the P-wave 3D velocity model with the embedded hanging wall LVB at 2 km elevation.....	86
Figure 4-2: P-wave travel-time plots for lines 1-4 from Behrendt et al. (1968).....	88
Figure 4-3: Line 2 gravity and seismic refraction interpretation reproduced from Behrendt et al. (1968).	90
Figure 4-4: S-wave velocity depth cross section A-B (see Figure 4-1).....	95
Figure 4-5: Radial-component JLDW seismogram from the M 1.4 normal-faulting earthquake on 19 April 2001.	96
Figure 4-6: Synthetic radial-component-seismogram record section for the 19 April 2001 earthquake.....	97
Figure 4-7: 2D ray-tracing slices through the 3D S-wave velocity model.....	98
Figure 4-8: S-wave velocity-depth cross section C-D (see Figure 4-1) used to model the 29 Sep. 1996 M 1.6 earthquake.	100
Figure 4-9: Line 4 traveltimes and interpretations reproduced from Behrendt et al. (1968).....	101
Figure 4-10: Radial-component JLDW observed seismogram from the M 1.6 normal-faulting earthquake on 29 Sep. 1996.....	102
Figure 4-11: S-wave velocity-depth cross section E-F (see Figure 4-1) used to model the 15 Nov. 2001 M 2.9 earthquake.	104
Figure 4-12: Observed and synthetic radial-component JLDW seismograms the M 2.9 normal-faulting earthquake on 15 Nov. 2001.....	105
Figure 4-13: (A) P-wave travel-time plot for lines 2 from Behrendt et al. (1968) and (B) corresponding slice of the 3D P-wave velocity model.107	
Figure 4-14: (A) Line 2 interpretation from Behrendt et al. (1968) and (B) corresponding slice of the 3D P-wave velocity model.	108
Figure 4-15: Plan view of the P-wave 3D velocity model with embedded Jackson Hole LVB at elevation 2 km.....	110
Figure 4-16: E15S horizontal component < 1 Hz 3D finite-difference RGF's moment-time	

histories at JLDW for a point-source at the northeast corner of the Teton fault	111
Figure 4-17: N15E horizontal component < 1 Hz 3D finite-difference RGF's moment-time histories at JLDW for a point-source at the northeast corner of the Teton fault	112
Figure 4-18: E15S horizontal component < 1 Hz 3D finite-difference RGF's moment-time histories at JLDW for a point-source at the southeast corner of the Teton fault	113
Figure 4-19: N15E horizontal component < 1 Hz 3D finite-difference RGF's moment-time histories at JLDW for a point-source at the southeast corner of the Teton fault	114
Figure 4-20: Simulated peak motion characteristics for a M 7.1 earthquake on the Teton fault.....	116
Figure 5-1: Jackson Lake Dam section showing locations of site response seismometers JLDW-JLD7.....	128
Figure 5-2: Profiles across Jackson Lake Dam at stations 12+00, 24+00, and 31+00 (Stelma, 1996) showing location of site response seismometers JLD2 through JLD6.....	129
Figure 5-3: Compressional and shear wave velocity profiles for the soil column underlying the north dike of Jackson Lake Dam, as determined by crosshole velocity measurements (Sirles, 1986).	130
Figure 5-4: M 3.2 earthquake located near Driggs Idaho.	136
Figure 5-5: M 3.1 earthquake located 34 km southeast of the Jackson Lake Dam in the Gros Ventre Range.....	137
Figure 5-6: Spectral ratios relative to JLDW for 29 earthquakes recorded by the RefTek instrumentation initially deployed at seven sites (JLDW through JLD7).	141
Figure 5-7: Spectral ratios relative to JLDW for 24 earthquakes recorded by the upgraded instrumentation deployed at sites JLDW, JLD2, JLD3, and JLD5... .	142
Figure 5-8: Spectral ratios relative to JLD3 for 29 earthquakes recorded by the initial deployment of RefTek instruments.....	144
Figure 5-9: Average spectral ratios relative to JLDW for 29 earthquakes recorded by the initial deployment of RefTek instruments	146
Figure 5-10: Average spectral ratios relative to JLDW for 29 earthquakes recorded by the upgraded instrumentation deployed at stations JLDW, JLD2, JLD3 and JLD5.....	147
Figure 5-11: (A) Unwrapped phase at JLD2 relative to JLDW for 7 representative earthquakes. (B) Impulse response functions constructed from the average spectral ratio, and from individual or average relative phases.	149
Figure 5-12: Tabas E-W acceleration and velocity waveforms (solid lines) convolved with several realizations of the JLD2 weak-motion impulse response functions (dashed lines).	150
Figure 5-13: (A) Unwrapped phase at JLD3 relative to JLDW for 7 representative earthquakes. (B) Impulse response functions constructed from the average spectral ratio, and from individual or average relative phases.	152
Figure 5-14: Tabas E-W acceleration and velocity waveforms (solid) convolved with several realizations of the JLD3 weak-motion impulse response functions	

(dashed).....	153
Figure 5-15: Bedrock input motions (solid lines), and bedrock motions convolved with JLD2 weak-motion response (dotted lines).	154
Figure 5-16: Bedrock input motions (solid lines), and bedrock motions convolved with JLD3 weak-motion response (dotted lines).	155
Figure 5-17: Bedrock input motions (left), and motions convolved with JLD2 weak-motion site response (right).....	157
Figure 5-18: Bedrock input motions (left), and motions convolved with JLD3 weak-motion site response (right).....	159
Figure 5-19: Simulation of Lomnitz et al.'s (1999) soil response.....	161
Figure 5-20: Simple 2D S-wave velocity model of the glacial scour basin beneath the dam	163
Figure 5-21: 1D S-wave velocity profile from the middle of the 2D glacial scour basin	164
Figure 5-22: Simple 2D S-wave Qs model of the glacial scour basin beneath the dam.....	165
Figure 5-23: Horizontal 2D finite-difference acceleration record section z = 0 m	166
Figure 5-24: Horizontal 2D finite-difference acceleration record section z = 10 m	168
Figure 5-25: Horizontal 2D finite-difference acceleration record section z = 20 m	169
Figure 5-26: Horizontal 2D finite-difference acceleration record section z = 30 m	170
Figure 5-27: Horizontal 2D finite-difference acceleration record section z = 40 m	171
Figure 5-28: Horizontal 2D finite-difference acceleration record section z = 50 m	172
Figure 5-29: Vertical 2D finite-difference acceleration record section z = 0 m.....	174
Figure 5-30: Vertical 2D finite-difference acceleration record section z = 10 m.....	175
Figure 5-31: Vertical 2D finite-difference acceleration record section z = 20 m.....	176
Figure 5-32: Vertical 2D finite-difference acceleration record section z = 30 m.....	177
Figure 5-33: Vertical 2D finite-difference acceleration record section z = 40 m.....	178
Figure 5-34: Vertical 2D finite-difference acceleration record section z = 50 m.....	179
Figure 6-1: Plan view of the ground motion P-wave 3D velocity model at elevation 2 km.	186
Figure 6-2: High-frequency approximation to the Kostrov slip-velocity function.....	192
Figure 6-3: Two cross sections of the ground motion P-wave 3D velocity model with orientations as labeled.....	196
Figure 6-4: Epicenters of the EGFs with P-wave 3D velocity model at elevation 2 km....	199
Figure 6-5: E15S-component S-wave normal-dip-slip polarities and 0.8-1.5 Hz amplitudes at JLDW for a 35° fault dip.....	201
Figure 6-6: N15E-component S-wave normal-dip-slip polarities and 0.8-1.5 Hz amplitudes at JLDW for a 35° fault dip.....	203
Figure 6-7: Vertical-component S-wave normal-dip-slip polarities and 0.8-1.5 Hz amplitudes at JLDW for a 35° fault dip.....	204
Figure 6-8: Low-frequency (< 1 Hz) E15S-component velocity waveforms for a full Teton fault rupture with a 35° fault dip.	208
Figure 6-9: Low-frequency (< 1 Hz) N15E-component velocity waveforms for a full Teton fault rupture with a 35° fault dip.209	
Figure 6-10: Low-frequency (< 1 Hz) vertical-component velocity waveforms for a full Teton fault rupture with a 35° fault dip.	210
Figure 6-11: Low-frequency (< 1 Hz) horizontal peak velocity, acceleration, and Arias intensity profiles for a full Teton fault rupture with a 35° dip (black curves)..	211
Figure 6-12: Low-frequency (< 1 Hz) E15S-component velocity waveforms for a full Teton fault rupture with a 60° fault dip.	213

Figure 6-13:	Low-frequency (< 1 Hz) N15E-component velocity waveforms for a full Teton fault rupture with a 60° fault dip.	214
Figure 6-14:	Low-frequency (< 1 Hz) vertical-component velocity waveforms for a full Teton fault rupture with a 60° fault dip.	215
Figure 6-15:	Low-frequency (< 1 Hz) horizontal peak velocity, acceleration, and Arias intensity profiles for a full Teton fault rupture with a 60° dip (black curves). ..	217
Figure 6-16:	JLDW rock site mean downstream horizontal PSA response spectra for a 35°-dipping northern Teton fault segment (solid).	219
Figure 6-17:	JLDW rock site 84% quantile downstream horizontal PSA response spectra for a 35°-dipping northern Teton fault segment (solid).....	220
Figure 6-18:	JLDW rock site PSA response spectra for a 35°-dipping northern Teton fault segment for all hypocenters.	222
Figure 6-19:	JLDW rock site central hypocenter PSA response spectra for a 35°-dipping northern Teton fault segment (black).....	223
Figure 6-20:	JLDW rock site northern hypocenter PSA response spectra for a 35°-dipping northern Teton fault segment (black).....	224
Figure 6-21:	JLDW rock site southern hypocenter PSA response spectra for a 35°-dipping northern Teton fault segment (black).....	225
Figure 6-22:	JLDW rock site PSA response spectra for a 45°-dipping northern Teton fault segment using all hypocenter positions.	227
Figure 6-23:	JLDW rock site mean downstream horizontal PSA response spectra for a 45°-dipping northern Teton fault segment (solid).	228
Figure 6-24:	JLDW rock site 84% quantile downstream horizontal PSA response spectra for a 45°-dipping northern Teton fault segment (solid).....	229
Figure 6-25:	JLDW rock site central hypocenter PSA response spectra for a 45°-dipping northern Teton fault segment (black).....	230
Figure 6-26:	JLDW rock site southern hypocenter PSA response spectra for a 45°- dipping northern Teton fault segment (black).	231
Figure 6-27:	JLDW rock site northern hypocenter PSA response spectra for a 45°- dipping northern Teton fault segment (black).	232
Figure 6-28:	JLDW rock site PSA response spectra for a 60°-dipping northern Teton fault segment using all hypocenter positions.	235
Figure 6-29:	JLDW rock site central hypocenter PSA response spectra for a 60°-dipping northern Teton fault segment (black).....	236
Figure 6-30:	JLDW rock site southern hypocenter PSA response spectra for a 60°- dipping northern Teton fault segment (black).	237
Figure 6-31:	JLDW rock site northern hypocenter PSA response spectra for a 60°- dipping northern Teton fault segment (black).	239
Figure 6-32:	JLDW rock site mean PSA horizontal response spectra for a 60°- dipping northern Teton fault segment.....	240
Figure 6-33:	JLDW rock site 84% quantile PSA horizontal response spectra for a 60°- dipping northern Teton fault segment.....	241
Figure 6-34:	JLDW rock site ratios of 35°-to-60°-dipping northern Teton fault segment PSA response spectra.....	242
Figure 6-35:	JLDW rock site ratios of 45°-to-60°-dipping northern Teton fault segment PSA response spectra.....	243

Figure 6-36:	JLDW rock site ratios of 35°-to-45°-dipping northern Teton fault segment PSA response spectra.....	244
Figure 6-37:	JLDW rock site PSA response spectra corresponding to the mean acceleration seismograms.....	251
Figure 6-38:	JLDW rock site mean acceleration seismograms for dynamic analyses of Jackson Lake Dam.....	252
Figure 6-39:	JLDW rock site mean velocity seismograms for dynamic analyses of Jackson Lake Dam.....	253
Figure 6-40:	JLDW rock site mean displacement seismograms for dynamic analyses of Jackson Lake Dam.....	254
Figure 6-41:	JLDW rock site PSA response spectra corresponding to the 84 percentile acceleration seismograms.....	255
Figure 6-42:	JLDW rock site 84 percentile acceleration seismograms for dynamic analyses of Jackson Lake Dam.....	256
Figure 6-43:	JLDW rock site 84 percentile velocity seismograms for dynamic analyses of Jackson Lake Dam.....	257
Figure 6-44:	JLDW rock site 84 percentile displacement seismograms for dynamic analyses of Jackson Lake Dam.....	258
Figure 6-45:	Lolleo, Chile, acceleration seismograms for dynamic analyses of the concrete section of Jackson Lake Dam.....	260
Figure 6-46:	Lolleo, Chile, velocity seismograms for dynamic analyses of Jackson Lake Dam.....	261
Figure 6-47:	Lolleo, Chile, displacement seismograms for dynamic analyses of Jackson Lake Dam.....	262
Figure 6-48:	Response spectra corresponding to the Lolleo acceleration seismograms.....	263
Figure 6-49:	East horizontal component microearthquake velocity seismograms for JLDW and JLD3.....	265
Figure 6-50:	Time-frequency for the JLDW east-component seismogram from Figure 6-49.....	266
Figure 6-51:	Time-frequency for the JLD3 east-component seismogram from Figure 6-49.....	267
Figure 6-52:	NOAH velocity-density depth model for the compaction region.....	269
Figure 6-53:	NOAH velocity-density depth model for the soil mix wall region.....	270
Figure 6-54:	Mean JLDW E15S rock motion velocity (a) and acceleration (b) convolved with the JLD3 soil response transfer function.....	272
Figure 6-55:	84% JLDW E15S rock motion velocity (a) and acceleration (b) convolved with the JLD3 soil response transfer function.....	273
Figure 6-56:	Tabas E15S rock motion velocity (a) and acceleration (b) convolved with the JLD3 soil response transfer function.....	274
Figure 6-57:	Time-domain compacted soil responses for JLD3 response input motions.....	276
Figure 6-58:	Compacted soil acceleration response spectra for JLD3 response input motions.....	277
Figure 6-59:	Time-domain compacted soil responses for rock response input motions.....	278
Figure 6-60:	Compacted soil acceleration response spectra for rock response input motions.....	279
Figure 6-61:	Time-domain soil mix wall responses for JLD3 response input motions.....	280

Figure 6-62:	SMW soil acceleration response spectra for JLD3 response input motions.....	281
Figure 6-63:	Time-domain soil mix wall responses for rock response input motions.	283
Figure 6-64:	SMW soil acceleration response spectra for rock response input motions.....	284
Figure 7-1:	Map view of the Imperial Valley area from Archuleta (1984).	293
Figure 7-2:	El Centro Array station E06 acceleration seismograms.	295
Figure 7-3:	El Centro Array station E06 velocity seismograms.....	297
Figure 7-4:	El Centro Array station E06 pseudo-acceleration response spectra.....	298
Figure 7-5:	El Centro Array station E07 acceleration seismograms.	299
Figure 7-6:	El Centro Array station E07 velocity seismograms.....	300
Figure 7-7:	El Centro Array station E07 pseudo-acceleration response spectra.....	301
Figure 7-8:	El Centro Array station EMO acceleration seismograms.	302
Figure 7-9:	El Centro Array station EMO velocity seismograms.	303
Figure 7-10:	El Centro Array station EMO pseudo-acceleration response spectra.....	304
Figure 7-11:	Plan view of observed peak velocities and accelerations from the M 6.7 1994 Northridge earthquake.	306
Figure 7-12:	S-wave velocity profile from a 3D randomization of a 2D velocity model for the top 2 km of the crust.....	310
Figure 7-13:	First example of a synthetic three-component SV scattering function.....	312
Figure 7-14:	Another example of a synthetic three-component SV scattering function.	313
Figure 7-15:	Effective stress distribution that produced the best-fitting Northridge ground motions.....	314
Figure 7-16:	Slip-velocity distribution that produced the best-fitting Northridge ground motions.....	315
Figure 7-17:	Rise-time distribution that produced the best-fitting Northridge ground motion	316
Figure 7-18:	Slip distribution that produced the best-fitting Northridge ground motion	317
Figure 7-19:	Fractional-rupture-velocity distribution that produced the best-fitting Northridge ground motion	319
Figure 7-20:	Rupture time distribution that produced the best-fitting Northridge ground motion	320
Figure 7-21:	Observed and simulated peak horizontal component velocities and accelerations as labeled for station RSS (Rinaldi).....	321
Figure 7-22:	Observed and simulated peak horizontal component velocities and accelerations as labeled for station SYL (Sylmar).....	322
Figure 7-23:	Observed and simulated peak horizontal component velocities and accelerations as labeled for station NHL (Newhall).....	323
Figure 7-24:	Observed and simulated peak horizontal component velocities and accelerations as labeled for station U56.	324
Figure 7-25:	Observed and simulated peak horizontal component velocities and accelerations as labeled for station PARD.....	325
Figure 7-26:	Observed and simulated peak horizontal component velocities and accelerations as labeled for station PDM (Pacoima Dam downstream station).	326
Figure 7-27:	Observed and best-fitting Northridge horizontal PSA response spectra.	327
Figure 7-28:	Statistical synthetic PSA results.	329
Figure 7-29:	Example of relative slip-velocity function.....	333

Figure 7-30:	Map showing the location of the regional EGF earthquakes relative to the dam.....	337
Figure 7-31:	Site JLDW velocity seismograms from the 21 Apr. 2001 M 5.2 Idaho earthquake.....	341
Figure 7-32:	Site JLDW Fourier velocity spectra from the 21 Apr. 2001 M 5.2 Idaho earthquake.....	342
Figure 7-33:	Site JLDW acceleration response spectra from the 21 Apr. 2001 M 5.2 Idaho earthquake.....	343
Figure 7-34:	Subevent sum M 7.1 northern Teton fault earthquake simulation JLDW vertical response before long-period correction.	344
Figure 7-35:	M 7.1 northern Teton fault earthquake simulation JLDW vertical response....	346
Figure 7-36:	Subevent sum M 7.1 northern Teton fault earthquake simulation JLDW north response before long-period correction.	347
Figure 7-37:	M 7.1 northern Teton fault earthquake simulation JLDW north response.	348
Figure 7-38:	Subevent sum M 7.1 northern Teton fault earthquake simulation JLDW east response before long-period correction.	349
Figure 7-39:	M 7.1 northern Teton fault earthquake simulation JLDW east response.	350
Figure 7-40:	Site JLDW velocity seismograms from the 24 Nov. 2000 M 4.6 Yellowstone earthquake.....	352
Figure 7-41:	Site JLDW Fourier velocity spectra from the 24 Nov. 2000 M 4.6 Yellowstone earthquake.....	353
Figure 7-42:	Site JLDW acceleration response spectra from the 24 Nov. 2000 M 4.6 Yellowstone earthquake.....	354
Figure 7-43:	Subevent sum M 7.1 northern Teton fault earthquake simulation JLDW vertical response before long-period correction.	356
Figure 7-44:	M 7.1 northern Teton fault earthquake simulation JLDW vertical response....	357
Figure 7-45:	Subevent sum M 7.1 northern Teton fault earthquake simulation JLDW north response before long-period correction.	358
Figure 7-46:	M 7.1 northern Teton fault earthquake simulation JLDW north response.	359
Figure 7-47:	Subevent sum M 7.1 northern Teton fault earthquake simulation JLDW east response before long-period correction.	360
Figure 7-48:	M 7.1 northern Teton fault earthquake simulation JLDW north response.	361
Figure 7-49:	Site JLD3 velocity seismograms from the 21 Apr. 2001 M 5.2 Idaho earthquake.....	363
Figure 7-50:	Site JLD3 Fourier velocity spectra from the 21 Apr. 2001 M 5.2 Idaho earthquake.....	364
Figure 7-51:	Site JLD3 acceleration response spectra from the 21 Apr. 2001 M 5.2 Idaho earthquake.....	365
Figure 7-52:	Subevent sum M 7.1 northern Teton fault earthquake simulation JLD3 vertical response before long-period correction.	367
Figure 7-53:	M 7.1 northern Teton fault earthquake simulation JLD3 vertical response.	368
Figure 7-54:	Subevent sum M 7.1 northern Teton fault earthquake simulation JLD3 north response before long-period correction.	369
Figure 7-55:	M 7.1 northern Teton fault earthquake simulation JLD3 north response.	370
Figure 7-56:	Subevent sum M 7.1 northern Teton fault earthquake simulation JLD3 east response before long-period correction.	371

Figure 7-57:	M 7.1 northern Teton fault earthquake simulation JLD3 east response	372
Figure 7-58:	Site JLD3 velocity seismograms from the 24 Nov. 2000 M 4.6 Yellowstone earthquake.....	374
Figure 7-59:	Site JLD3 Fourier velocity spectra from the 24 Nov. 2000 M 4.6 Yellowstone earthquake.....	375
Figure 7-60:	Site JLD3 acceleration response spectra from the 24 Nov. 2000 M 4.6 Yellowstone earthquake.....	376
Figure 7-61:	Subevent sum M 7.1 northern Teton fault earthquake simulation JLD3 vertical response before long-period correction.	377
Figure 7-62:	M 7.1 northern Teton fault earthquake simulation JLD3 vertical response.	378
Figure 7-63:	Subevent sum M 7.1 northern Teton fault earthquake simulation JLD3 north response before long-period correction.	379
Figure 7-64:	M 7.1 northern Teton fault earthquake simulation JLD3 north response	380
Figure 7-65:	Subevent sum M 7.1 northern Teton fault earthquake simulation JLD3 east response before long-period correction.	381
Figure 7-66:	M 7.1 northern Teton fault earthquake simulation JLD3 north response	382
Figure 7-67:	Epicenters of the three "broadband" EGF local earthquakes with P-wave 3D velocity model at elevation 2 km.	384
Figure 7-68:	Site JLDW velocity seismograms and Fourier spectra from the M 2.9 11 July 1998 earthquake	385
Figure 7-69:	Site JLDW velocity seismograms and Fourier spectra from the M 3.2 20 November 2002 earthquake	386
Figure 7-70:	Site JLDW velocity seismograms and Fourier spectra from the M 3.7 29 January 2002 earthquake	387
Figure 7-71:	Focal mechanism for the M 2.9 EGF on 11 July 1998.....	388
Figure 7-72:	JLDW 84% quantile acceleration response spectra for the 11 July 1998 EGF	389
Figure 7-73:	JLDW velocity seismograms for the best-fitting 84% quantile acceleration response spectra for the 11 July 1998 EGF	390
Figure 7-74:	JLDW acceleration seismograms for the best-fitting 84% quantile acceleration response spectra for the 11 July 1998 EGF	391
Figure 7-75:	JLDW displacement seismograms for the best-fitting 84% quantile acceleration response spectra for the 11 July 1998 EGF	392
Figure 7-76:	JLDW mean and 84% quantile northern Teton fault segment acceleration response spectra using the M 3.2 20 Nov. 2002 EGF	394
Figure 7-77:	JLDW 84% quantile acceleration response spectra for the 20 Nov. 2002 EGF	395
Figure 7-78:	JLDW velocity seismograms for the best-fitting 84% quantile acceleration response spectra for the 20 Nov. 2002 EGF	396
Figure 7-79:	JLDW acceleration seismograms for the best-fitting 84% quantile acceleration response spectra for the 20 Nov. 2002 EGF	398
Figure 7-80:	JLDW displacement seismograms for the best-fitting 84% quantile acceleration response spectra for the 20 Nov 2002 EGF	399
Figure 7-81:	JLDW PSA ratios of the M 3.2 EGF ground motions to the M 2.9 EGF ground motions	400
Figure 7-82:	JLDW PSA ratios of the M 3.7 EGF ground motions to the M 2.9 EGF	

ground motions	402
Figure 7-83: JLDW rock site mean downstream horizontal PSA response spectra for a 35°-dipping northern Teton fault segment (solid).....	404
Figure 7-84: JLDW rock site hybrid Section 6 84% quantile downstream horizontal PSA response spectra for a 35°-dipping northern Teton fault segment (solid).....	405
Figure 7-85: JLDW rock site hybrid Section 6 PSA response spectra for a 35°-dipping northern Teton fault segment for all hypocenters.....	406
Figure 7-86: Schematic plan and cross section views of the low-velocity basin boundary configuration for Jackson Lake Dam.....	407
Figure 7-87: Differential displacements between sites JLD3 and JLD2 for a M 7.1 northern Teton fault segment earthquake.	415
Figure 8-1: Mean downstream horizontal JLDW rock site PSA response spectra for a 35°-dipping northern Teton fault segment (solid).....	429
Figure 8-2: 84% quantile downstream horizontal JLDW rock site PSA response spectra for a 35°-dipping northern Teton fault segment (solid).....	430
Figure 8-3: Mean downstream horizontal JLDW rock site PSA response spectra for a 45°-dipping northern Teton fault segment (solid).....	431
Figure 8-4: 84% quantile downstream horizontal JLDW rock site PSA response spectra for a 45°-dipping northern Teton fault segment (solid).....	432
Figure 8-5: Mean JLDW rock site PSA horizontal response spectra for a 60°-dipping northern Teton fault segment.	433
Figure 8-6: 84% quantile JLDW rock site PSA horizontal response spectra for a 60°-dipping northern Teton fault segment.....	434
Figure 8-7: Northern Teton fault segment mean rock synthetic ground motion acceleration time histories.	438
Figure 8-8: Northern Teton fault segment mean rock synthetic ground motion velocity time histories.....	439
Figure 8-9: Northern Teton fault segment mean rock synthetic ground motion displacement time histories.....	440
Figure 8-10: Northern Teton fault segment mean rock synthetic ground motion acceleration response spectra.....	441
Figure 8-11: Northern Teton fault segment 84% quantile rock synthetic ground motion acceleration time histories.....	442
Figure 8-12: Northern Teton fault segment 84% quantile rock synthetic ground motion velocity time histories.....	443
Figure 8-13: Northern Teton fault segment 84% quantile rock synthetic ground motion displacement time histories.	444
Figure 8-14: Northern Teton fault segment 84% quantile rock synthetic ground motion acceleration response spectra.	445
Figure 8-15: Llolleo Valparaiso, Chile, proxy for a Northern Teton fault segment rock ground motion acceleration time histories.....	446
Figure 8-16: Llolleo Valparaiso, Chile, proxy for a Northern Teton fault segment rock ground motion velocity time histories.	447
Figure 8-17: Llolleo Valparaiso, Chile, proxy for a Northern Teton fault segment rock ground motion displacement time histories.	448

Figure 8-18: Llolleo Valparaiso, Chile, proxy for a Northern Teton fault segment rock ground motion acceleration response spectra 449

List of Tables

<u>Table No.</u>	<u>Title</u>	<u>Page</u>
Table 2-1:	Teton Fault - Event Data.....	35
Table 2-2:	Teton Fault Rupture Scenario Summary	40
Table 3-1:	Station corrections from the hypocenter-velocity-station correction inversion.....	48
Table 3-2:	Number of Different Focal Mechanisms for < 5° T-axis Azimuth Variability.....	56
Table 3-3:	Number of Different Focal Mechanisms for < 20° T-axis Azimuth Variability.....	56
Table 3-4a:	Completeness Periods and Event Counts Used in Recurrence Calculations, JLSN Catalog	73
Table 3-4b:	Completeness Periods and Event Counts Used in Recurrence Calculations, JLSN and 1963-1986 Catalog	73
Table 3-5a:	Recurrence Parameters, JLSN Catalog.....	76
Table 3-5b:	Recurrence Parameters, Combined Catalogs.....	76
Table 3-6a:	JLSN Catalog: Return Periods, Observed and Maximum Likelihood, with Upper and Lower Bounds at 95% Confidence	77
Table 3-6b:	Combined Catalogs: Return Periods, Observed and Maximum Likelihood, with Upper and Lower Bounds at 95% Confidence	77
Table 4-1:	Best-Estimates of Relationships between P-wave Velocity and Vs, r, Qp, and Qs	93
Table 5-1:	RefTek Data Collection Summary.....	135
Table 6-1:	Empirical Green's Function Earthquake Information	198
Table 6-2:	JLDW Rock Ground Motion Parameters: 35°-Dipping Northern Teton Fault Segment.....	218
Table 6-3:	JLDW Rock Ground Motion Parameters: 45°-Dipping Northern Teton Fault Segment	226
Table 6-4:	JLDW Rock Ground Motion Parameters: 60°-Dipping Northern Teton Fault Segment	234
Table 6-5:	Ground Motion Input Scenarios for Nonlinear Soil Calculations	268
Table 7-1:	Regional EGF Earthquake Locations	335
Table 7-2:	21 April 2001 EGF Focal Mechanism Nodal Plane Estimates.....	336
Table 7-3:	Regional EGF Earthquake Simulation Parameters	340
Table 7-4:	Local Broadband Empirical Green's Function Earthquake Information.....	373
Table 7-5:	JLDW Rock Ground Motion Parameters: 35°-Dipping Northern Teton Fault Segment	401
Table 8-1:	Ground Motion Parameters for a 35°-Dipping Northern Teton Fault Segment.....	427
Table 8-2:	Ground Motion Parameters for a 45°-Dipping Northern Teton Fault Segment.....	428
Table 8-3:	Ground Motion Parameters for a 60°-Dipping Northern Teton Fault Segment.....	428
Table 8-4:	Rock PHA for the Concrete Section, PHA Range 1.....	436
Table 8-5:	Rock PHA for the Concrete Section, PHA Range 2.....	437
Table 8-6:	Ground Motion Time History Annual Exceedence Probabilities	450

Appendices

<u>Appendix</u>	<u>Title</u>
A	Teton Fault Section and Fault Scarp Slip Rate Data
B	Hypocenter-Velocity-Station Correction Inversion
C	3D P-Wave Velocity Model Plots
D	3D Empirical Green's Function Plots
E	3D Nonlinear Soil Response Plots
F	Final Report - Nonlinear Wave Propagation in One and Two Dimensions - by R.J. Archuleta and Kenichi Tsuda
G	Review Comments by Dr. Paul Somerville

Plates

- 1 Partial reproduction of the gravity, geologic and seismic refraction map from Behrendt et al. (1968).